Journal of Anatomy

J. Anat. (2014) **224**, pp377–391 doi: 10.1111/joa.12154

Distribution of the hematopoietic growth factor G-CSF and its receptor in the adult human brain with specific reference to Alzheimer's disease

Sami Ridwan,* Henrike Bauer, Katrin Frauenknecht, Kyra Hefti, Harald von Pein and Clemens J. Sommer

Department of Neuropathology, University Medical Center of the Johannes Gutenberg University Mainz, Mainz, Germany

Abstract

The granulocyte colony-stimulating factor (G-CSF), being a member of the hematopoietic growth factor family, is also critically involved in controlling proliferation and differentiation of neural stem cells. Treatment with G-CSF has been shown to result in substantial neuroprotective and neuroregenerative effects in various experimental models of acute and chronic diseases of the central nervous system. Although G-CSF has been tested in a clinical study for treatment of acute ischemic stroke, there is only fragmentary data on the distribution of this cytokine and its receptor in the human brain. Therefore, the present study was focused on the immunohistochemical analysis of the protein expression of G-CSF and its receptor (G-CSF R) in the adult human brain. Since G-CSF has been shown not only to exert neuroprotective effects in animal models of Alzheimer's disease (AD) but also to be a candidate for clinical treatment, we have also placed an emphasis on the regulation of these molecules in this neurodegenerative disease. One major finding is that both G-CSF and G-CSF R were ubiquitously but not uniformly expressed in neurons throughout the CNS. Protein expression of G-CSF and G-CSF R was not restricted to neurons but was also detectable in astrocytes, ependymal cells, and choroid plexus cells. However, the distribution of G-CSF and G-CSF R did not substantially differ between AD brains and control, even in the hippocampus, where early neurodegenerative changes typically occur.

Key words: Alzheimer's disease; granulocyte colony-stimulating factor; granulocyte colony-stimulating factor receptor; immunohistochemistry; neurotrophin.

Introduction

Since neurotropic growth factors such as the nerve growth factor (NGF) or brain-derived neurotrophic factor (BDNF) are well known to play a key role in neuronal differentiation and survival, the induction of endogenous neurotrophic factors as well as application of exogenous neurotrophins have convincingly been demonstrated to protect neurons against a variety of injuries (Hennigan et al. 2007). Over the past years, it has become clear that hematopoietic growth factors such as erythropoietin (EPO), granulocyte-monocyte colony-stimulating factor (GM-CSF), and granulocyte colony-stimulating factor (G-CSF) are also potent neuroprotectants and potential candidates for the treatment of various neurological diseases in humans (Maurer et al. 2008). Within the family of hematopoeitic growth factors, G-CSF has been shown in a series of experimental stroke studies to protect against ischemic damage and enhance the neurological outcome (Minnerup et al. 2008). Since it was demonstrated that the G-CSF receptor (G-CSF R) is widely expressed in the central nervous system (CNS) of mice and rats, it is reasonable to assume that these protective effects are mediated by this receptor (Schäbitz et al. 2003; Schneider et al. 2005). Furthermore, G-CSF is also expressed within the brain, which points to a possible autocrine loop (Schneider et al. 2005). After cerebral ischemia, in accordance with findings from rodents, both G-CSF and G-CSF R are upregulated also in the human brain (Hasselblatt et al. 2007). However, to our knowledge, no systematic analysis of the distribution of G-CSF and its receptor within the human brain has existed up to now. Thus, with regard to multicenter trials evaluating the effect of G-CSF in acute stroke, as well as pilot clinical trials for the subacute phase of stroke that are already underway, it is imperative to fill

Correspondence
Clemens J. Sommer, Department of Neuropathology, University Medical Center of the Johannes Gutenberg University Mainz, 55131 Mainz, Germany. T: + 49 6131 173213; F: + 49 6131 176606; E: clemens.sommer@unimedizin-mainz.de

* *Present address: Department of Neurosurgery, University Medical Center Bonn, 53127, Bonn, Germany.*

Accepted for publication *2 December 2013*
Article published online *5 January 2014*

this gap in information. Furthermore, there is evidence from transgenic mouse models of Alzheimer's disease (AD) that G-CSF may also rescue memory impairment (Tsai et al. 2007). Recently, when immunohistochemically analyzing the distribution of GM-CSF and the major binding α-subunit of its receptor in the adult human brain and in AD brains, we were able to demonstrate a reduction of the GM-CSF receptor alpha (Rα) in the hippocampus which has been hypothesized to contribute to the progressive course of neurodegeneration in AD (Ridwan et al. 2012). Our present study has been designed to systematically analyze the distribution of G-CSF and its receptor within the forebrain, cerebellum, and brainstem of non-demented control brains and compare the respective pattern and intensity of immunoreactivity (IR) with brains from AD patients.

Material and methods

Brain samples and tissue preparation

All experiments were performed on the same series of postmortem brain tissues as previously published (Ridwan et al. 2012). Brains originated from three control subjects (one female, two males) with no history of any neurological or psychiatric disease and from six patients (three females and three males, respectively) clinically as well as neuropathologically diagnosed with AD (Table 1). The respective material was retrieved from the archives of the Department of Neuropathology at the University Medical Center of the Johannes Gutenberg University in Mainz, Germany, and the protocols were approved by the local Ethics Committees. The brains were immersion-fixed in 4% buffered formalin for about 2 weeks. Postmortem delay until fixation was 48 h at the most. Tissue samples containing neocortex, entorhinal cortex, basal ganglia, thalamus, hypothalamus, amygdala, hippocampus, cerebellum and brainstem were paraffin-embedded and cut into 4-μm-thick sections on a microtome. Histopathological diagnosis was performed using hematoxylin and eosin-stained sections. Staging of AD was based on neurofibrillary pathology as determined by immunohistochemical detection of hyperphosphorylated tau with the AT8 antibody (Mercken et al. 1992; Goedert et al. 1995), according to the protocol by Braak et al. (2006). Hippocampal sections were additionally stained with an antibody against β-amyloid.

Table 1 Clinical data.

No.	Sex	Age (years)	Braak-Staging	Cause of death
1	Female	52	Control	Hemorrhagic shock
2	Male	75	Control	Respiratory failure
3	Male	50	Control	Cardiorespiratory failure
4	Female	76	III–IV	Heart failure
5	Female	78	III–IV	Multiple organ failure
6	Female	83	III–IV	Heart failure
7	Male	72	III–IV	Multiple organ failure
8	Male	78	III–IV	Heart failure
9	Male	83	III–IV	Heart failure

Immunohistochemistry

Immunohistochemistry was performed on 4-μm-thick sections, using polyclonal rabbit antisera against G-CSF (sc-13102) and G-CSF R (sc-694) obtained from Santa Cruz (Santa Cruz Biotech Inc., Santa Cruz, CA, USA) as well as monoclonal mouse antibodies against PHF-tau (AT8) and β-amyloid (Clone 6F/3D) obtained from Pierce Biotechnology (Rockford, IL, USA and Dako (DakoCytomation, Glostrup, Denmark), respectively. For antigen retrieval, sections were boiled in citrate buffer (pH 9.0) for 20 min followed by a pretreatment with 1% hydrogen peroxide in Tris buffer (TBS) to inhibit endogenous peroxidase activity. Then, sections were incubated with the primary antibodies (G-CSF 1 : 100, G-CSF R 1 : 100) in TBS with 0.2% bovine serum albumin overnight at 4 °C. Incubation with the primary mouse antibodies (PHF-tau 1 : 1000, β-amyloid 1 : 100) was performed in Dako REAL Antibody Diluent (DakoCytomation) for 30 min at room temperature. This was followed by the secondary Biotin-SP-conjugated anti-rabbit antibody (Jackson ImmunoResearch Laboratories Inc., West Grove, PA, USA) for 20 min at room temperature or EnVision Flex-Mouse (Dako DM824) for 15 min at room temperature, respectively. After rinsing with phosphate-buffered saline + Tween (PBST), immunoreactivity (IR) was visualized by the avidin–biotin complex method (Vectastain, Vector Laboratories, Burlingame, CA, USA) or by incubation in EnVision (DakoCytomation), respectively. Immunohistochemistry against G-CSF R, PHF-tau and β-amyloid was performed using an automated staining system (Dako Autostainer Plus from DakoCytomation, Carpinteria, CA, USA). All sections were counterstained with hematoxylin. Negative control sections were treated with buffer replacing the primary antibodies and resulted in no staining (not shown). Classification of AD stages was performed by C.J.S.

Brain regions and semi-quantitative analysis

G-CSF and G-CSF R IR were studied in the following brain regions: cerebral neocortex (frontal, temporal, occipital, Wernicke's area), cingulated gyrus, hippocampus, basal ganglia (caudate nucleus, putamen, pallidum), thalamus and hypothalamus, subthalamus, claustrum and basal nucleus of Meynert, amygdala, cerebellum and the brainstem including midbrain, pons and medulla oblongata.

Within sections from these regions the respective areas were microscopically investigated. To get an overview of the density of labeled structures as well as of the intensity of immunostaining, the respective regions were semiquantitatively analyzed according to the protocol concerning the analysis of BDNF IR in the human brain by Murer et al. (1999), but with minor modifications as recently published by Ridwan et al. (2012). Thus, a simple three-stage score system was used to describe the density (+: low *or* < 10% labeled; ++: moderate *or* > 10% but < 50% labeled; +++: abundant *or* more than 50% labeled) and intensity (+: faint; ++: moderate; +++: strong) of immunostaining for both G-CSF and G-CSF R. Analysis was performed by S.R. who was blinded to the two groups. The spectrum of the variation within the groups is indicated within the tables.

To avoid any misinterpretations due to differences in the neuronal cell number between AD and control brains, we quantified the neuronal cell densities in the entorhinal cortex, the pyramidal layer of the hippocampal subfields CA1 to CA4 (hilus), and the granular layer of the dentate gyrus (DG), as well as in the subiculum which

includes all stage III/IV defining areas of AD. For this purpose, the respective regions were scanned at a magnification of ×20 with a Leica microscope (Leica, Germany), digitized and then transferred to a computer screen. Viable neurons on two adjacent regions per area strictly localized in the entorhinal cortex, within the pyramidal cell layer of the subiculum and CA1 to CA4 or in four regions strictly located in the granular layer of the DG, respectively, were quantified using the image processing and analysis program IMAGEJ (National Institutes of Health, Bethesda, MD, USA). In brief, neurons were identified within each photograph using small boxes of 100 μm edge length. Neurons in each box were manually marked, cell densities were calculated and expressed as mean neuronal cell number per mm^2 ('neuronal density') ± SEM. The Shapiro–Wilk test was used to verify normal distribution of the data to justify the use of a parametric or non-parametric test. Due to normal distribution of the data a Student *t*-test was used for the statistical analysis of means. A P value of < 0.05 was considered statistically significant. All statistical analysis was performed using the general statistics module of Analyse-it™ for MICROSOFT EXCEL (Analyse-it Software, Ltd., Leeds, UK). All data are expressed as mean ± standard error of mean (SEM).

Results

Patients

The median age of the control subjects was 59 years (ranging from 50 to 75 years) and the age of the AD patients averaged 78 years (ranging from 72 to 83 years; for further details see Table 1). All AD patients could be classified as stage-III to -IV cases, based on the respective distribution of neurofibrillary pathology (Braak et al. 2006).

Hippocampal neuronal cell densities

Quantitative analysis of neuronal cell densities in the subiculum, hippocampal pyramidal layers of CA1 to CA4 (hilus), the granular layer of the DG as well as the entorhinal cortex revealed no significant differences between control and AD brains ($P > 0.05$; Table 2).

Cellular distribution of G-CSF IR

In general, G-CSF IR was detectable in neuronal cell bodies, proximal dendrites, and axons throughout the CNS. Labeling of neuronal cell bodies was observed in the cytoplasm in the form of a fine granular pattern. In many regions, not all of the cells were stained and, in some regions, a variation in the staining intensity was observed insofar as strongly stained cells were frequently observed next to barely stained ones. Furthermore, cytoplasm and processes of astrocytes showed weak to moderate immunostaining throughout the CNS. Cells of the choroid plexus revealed a high density of weak to mostly moderately stained cells. Many ependymal cells also displayed faint to moderate IR (Table 1, Fig. 1).

Spatial distribution of G-CSF IR

Cerebral cortex

Weakly stained neurons with pyramidal morphology were present in all cortical regions analyzed (cf. Tables 3–6). They were preferentially located in layer III and showed a more intense staining in Wernicke's area, inferior temporal gyrus (Fig. 2), and cingulate gyrus, compared with the remaining cortical areas. Non-pyramidal neurons were also labeled, especially in layer I. Neuropil immunostaining was accentuated in layer I, but generally only weak throughout the remaining layers, with the exception of the cingulated gyrus, which showed a more pronounced neuropil immunostaining in layers V and VI.

Hippocampus

Neuronal cell bodies of the pyramidal layer in subfields CA1 to CA3 displayed faint immunostaining. Weak immunostaining was also detected in granule cells of the dentate gyrus. The density of immunoreactive neurons was higher in the pyramidal layer than in the granule cell layer of the dentate gyrus. Hilar neurons as well as neurons of the entorhinal cortex and the subiculum exhibited moderate labeling intensity. The neuropil was only weakly stained throughout all hippocampal regions.

Basal ganglia

Within the putamen and caudate nucleus, the intensity of neuronal G-CSF IR was weak. Most of the labeled cells in the putamen were large neurons, whereas small neurons remained almost completely unstained. The neuropil was slightly stained in both putamen and caudate nucleus, whereas some fiber bundles were more intensely labeled. In the pallidum, neurons were moderately labeled, whereas the neuropil disclosed only low levels of staining intensity.

Thalamus and hypothalamus

In general, all thalamic nuclei investigated showed distinct cytoplasmic G-CSF immunostaining of numerous neurons.

Table 2 Hippocampal neuronal densities.

	Subiculum	CA1	CA2	CA3	Hilus	DG	Entorhinal Cx
Control	26.6 ± 1.5	33.5 ± 1.2	37.2 ± 2.3	27.9 ± 0.9	20.6 ± 1.8	257.6 ± 8.8	24.0 ± 1.2
AD	25.6 ± 1.9	31.6 ± 0.8	35.1 ± 2.2	36.2 ± 3.4	23.8 ± 1.9	273.0 ± 1.6	29.9 ± 2.0

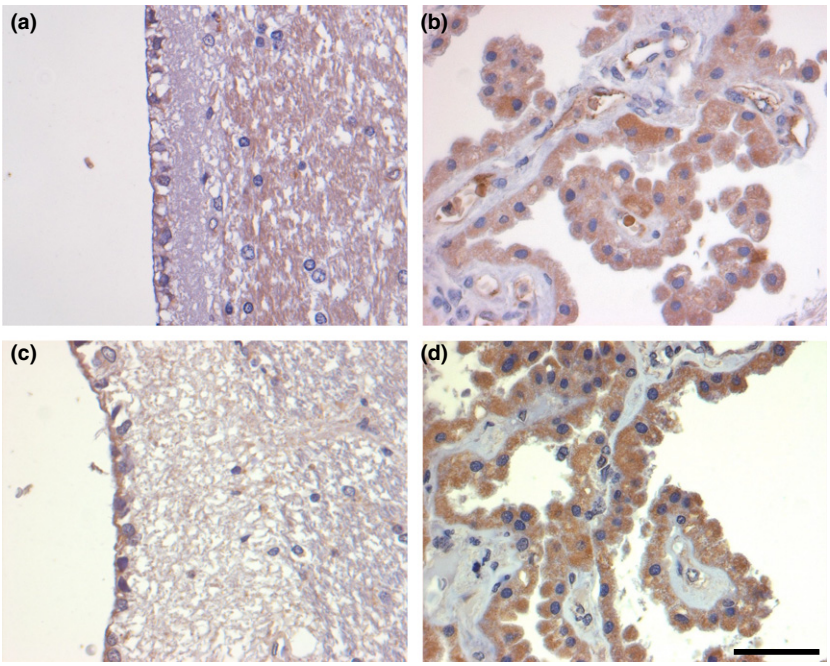

Fig. 1 G-CSF and G-CSF R IR in ependymal cells (a and c, respectively) and cells of the choroid plexus (b and d, respectively) of control brains. There is only faint G-CSF IR in ependymal cells (a), whereas staining for the G-CSF R is stronger (c). The choroid plexus reveals faint to moderate labeling for the ligand (b), whereas, again, staining for the receptor is slightly more intense (d). Sections are counterstained with hematoxylin. Scale bar: 50 μm.

Anterior, ventral lateral, dorsomedial, and subthalamic nuclei as well as the lateral pulvinar were slightly stained. A more intense neuronal IR was detectable in the ventral anterior nucleus and medial pulvinar. In general, the neurons in the hypothalamus were only weakly labeled. Neuropil staining was absent or very weak.

Claustrum and nucleus basalis of Meynert

Within the claustrum, up to 50% of neurons were faintly labeled. The neuropil was only slightly stained. Nearly all of the large neurons located in the nucleus basalis of Meynert were faintly stained, whereas no fibers with IR were detectable (Fig. 2).

Amygdala

There were numerous slightly stained neurons in the basolateral and basomedial nucleus, whereas the neurons of the lateral nucleus were more prominently stained. The neuropil was weakly stained in all three amygdaloid nuclei.

Cerebellum

Only a few cell bodies of the Purkinje cells were faintly labeled. Neurons of the molecular layer did not show any staining at all. Up to 50% of granule cell neurons were moderately labeled. Furthermore, a few scattered cells in the white matter were slightly to moderately stained. The dentate nucleus showed numerous faintly labeled neurons. The neuropil was only weakly stained (Fig. 2).

Brainstem

The neuromelanin-containing neurons of the substantia nigra, surrounded by a high density of faintly labeled fibers, exhibited no immunostaining at all. Numerous neurons of the red nucleus were faintly stained and fibers in this region also showed slight immunostaining. Within the mammillary bodies, numerous neurons were slightly stained. Similarly, most fibers also showed weak G-CSF staining. The diencephalic nuclei analyzed, i.e. oculomotor and trochlear nuclei, revealed a high density of moderately stained neuronal cell bodies and slightly to moderately stained fibers.

Within the pons, faint staining of neurons and the neuropil was observed in the pontine nuclei. Immunostaining was completely absent in the neurons and surrounding neuropil of the locus coeruleus. Motor neurons in the facial nucleus were weakly to moderately stained, whereas motor neurons of the trigeminal motor nucleus showed only weak IR. Surrounding fibers exhibited only a slight immunosignal.

In the inferior olivary complex, moderate IR could be observed in most neuronal cell bodies (Fig. 2). Neurons of the nucleus of the solitary tract as well as the adjacent neuropil displayed weak immunostaining. Neurons of the spinal trigeminal nucleus revealed abundant faintly labeled neuronal cell bodies embedded in moderately stained fibers.

Within neurons of the hypoglossal nucleus, a high density of moderately stained cell bodies could be observed. Fibers showed only weak IR. The vestibular nuclei disclosed moderately stained cell bodies next to slightly stained ones. Fibers were weakly labeled.

G-CSF IR in the brains of AD patients vs. controls

Throughout the various regions investigated in the CNS, the pattern and intensity of G-CSF IR was rather similar, both in control and AD brains (cf. Tables 3–6). However,

Table 3 Distribution of G-CSF IR in cortical regions.

	Control				AD			
	Neuronal cell bodies		Fibers		Neuronal cell bodies		Fibers	
	Density	Intensity	Density	Intensity	Density	Intensity	Density	Intensity
Cerebral cortex								
Wernicke's area								
I	++	+	++	+	0/++	0/++	0/++	0/++
II	0/+	0/+	0/++	0/+	0	0	0/++	0/+
III	++	+	0/++	0/+	++	+	0/++	0/+
IV	0	0	0/++	0/+	0	0	0/++	0/+
V	0/++	0/+	0/++	0/+	0/++	0/+	0/++	0/+
VI	0	0	0/++	0/+	0/+	0/+	0/++	0/+
Frontal pole								
I	++	+	0/+++	0/+	0/++	0/++	+/++	+
II	0	0	0/+++	0/+	0/+	0/+	+/++	+
III	0/++	0/+	0/+++	0/+	+/++	+	+/++	+
IV	0/+	0/+	0/+++	0/+	0/+	0/+	+/++	+
V	0/++	0/+	0/+++	0/+	0/+	0/+	+/++	+
VI	0/++	0/+	0/+++	0/+	0/+	0/+	+/++	+
Occipital pole								
I	++	+	0/++	0/++	0/++	0/++	0/++	0/+
II	0/+	0/+	0/++	0/+	0/+	0/+	0/++	0/+
III	0/+	0/+	0/++	0/+	0/++	0/+	0/++	0/+
IV	0/+	0/+	0/++	0/+	0/+	0/+	0/++	0/+
V	0	0	0/++	0/+	0/+	0/+	0/++	0/+
VI	0/+	0/+	0/++	0/+	0/+	0/+	0/++	0/+
Inferior temporal gyrus								
I	++	+/++	0/++	0/+	++	+/++	0/++	0/+
II	0/++	0/+	0/++	0/+	0/+	0/+	0/++	0/+
III	++	+	0/++	0/+	++	+	0/++	0/+
IV	0/+	0/+	0/++	0/+	0/+	0/+	0/++	0/+
V	0/++	0/+	0/++	0/+	0/++	0/+	0/++	0/+
VI	0/++	0/+	0/++	0/+	0/++	0/+	0/++	0/+
Cingulate gyrus								
I	+	+	0	0	++	+	0/+	0/+
II	0	0	0	0	0	0	0/+	0/+
III	++	+	0	0	0/++	0/+	0/+	0/+
IV	0	0	0	0	0	0	0/+	0/+
V	+	+	+	+	0/++	0/+	0/+	0/+
VI	0	0	+	+	0/++	0/+	0/+	0/+

Density: 0: no immunoreactive structures, + up to 10%, ++ 10–50%, +++ more than 50%. Intensity: 0: no immunoreactivity, + faint, ++ moderate, +++ strong. The range of minimum and maximum staining between individual cases is given.

there was some variation in staining intensity in all brain regions, with neuronal or neuropil staining dominating sometimes in control brains, sometimes in AD brains.

The same holds true when focusing on the hippocampus as a target structure in AD. Whereas G-CSF staining was completely absent in CA1 of AD brains, some weakly stained pyramidal cells were present in CA1 of controls. Neurons containing neurofibrillary tangles did not stain differently compared with surrounding neurons without tangles. Neither neurofibrillary tangles nor amyloid plaques disclosed G-CSF IR.

Cellular distribution of G-CSF R IR

G-CSF R IR was detectable in neuronal cell bodies, proximal dendrites, and axons throughout the CNS. Analogous to G-CSF IR, labeling in neuronal cell bodies was observed in the cytoplasm in the form of a finely granular pattern. The intensity of G-CSF R IR differed substantially within certain regions, with strongly stained cells next to very weakly stained ones. Astrocytes showed a faint to moderate intensity of IR in all regions of the CNS. The majority of ependymal cells exhibited a moderate intensity of G-CSF R IR

Table 4 Distribution of G-CSF IR in non-cortical areas of the forebrain.

	Control				AD			
	Neuronal cell bodies		Fibers		Neuronal cell bodies		Fibers	
	Density	Intensity	Density	Intensity	Density	Intensity	Density	Intensity
Basal ganglia								
Claustrum	++	+	0/++	0/+	0/+++	0/++	0/++	0/+
Putamen	0/+	0/+	0/++	0/+	0/+	0/+	+/++	+
Pallidum	++	++	0/++	0/+	0/++	0/+	0/++	0/+
Caudate nucleus	0/++	0/+	0/++	0/+	0/++	0/+	0/++	0/+
Basal nucleus of Meynert	++	+	0	0	++/+++	+	0/++	0/+
Hippocampus								
Dentate gyrus	0/+	0/+	0	0	0/+	0/+	0/++	0/+
Hilus	++	+	0/++	0/+	++	+	0/++	0/+
CA3	0/++	0/+	0/++	0/+	0/++	0/+	0/++	0/+
CA2	++	+	0/++	0/+	0/++	0/+	0/++	0/+
CA1	0/++	0/+	0	0	0	0	0/+	0/+
Subiculum	++	+/++	0/++	0/+	0/++	0/+	0/++	0/+
Entorhinal cortex	++	+/++	0/++	0/+	0/++	0/++	0/+	0/+
Lateral geniculate nucleus	++/+++	++	0/++	0/++	++/+++	+/++	0/++	0/++
Thalamus								
Anterior nucleus	++	+	0/+	0/+	0/++	0/++	0/++	0/+
Ventral anterior nucleus	++	+/++	++	+	0/+++	0/++	0/++	0/+
Ventral lateral nucleus	++/+++	+	0/++	0/+	++/+++	+/++	0/++	0/+
Dorsomedial nucleus	0/+++	0/+	0/+	0/+	0/+++	0/++	0/++	0/+
Subthalamic nucleus	++	+	0/++	0/+	0/+++	0/++	0/++	0/+
Pulvinar medial	++/+++	+/++	0/++	0/+	0/+++	0/+	0/++	0/+
Lateral	++	+	0/++	0/+	++	+	+/++	+
Hypothalamus								
Paraventricular nucleus	0/++	0/+	0	0	0/++	0/+	0/+	0/+
Supraoptic nucleus	0	0	0	0	0/+++	0/++	0/+	0/+
Dorsomedial nucleus	++/+++	+	0	0	+/++	+/++	0/++	0/+
Substantia nigra	0	0	0/++	0/+	0	0	0/++	0/+
Nucleus ruber	+++	+	0/++	0/+	++/+++	+/++	0/++	0/+
Mamillary bodies	0/++	0/+	0/++	0/+	0/+/++	0/+	0/++	0/+
Cerebellum								
Purkinje layer	0/+	0/+	–	–	0/+	0/+	–	–
Molecular layer	0	0	0/++	0/+	0/+	0/+	0/++	0/+
Granular layer	0/++	0/++	0/++	0/+	0/+	0/++	0/++	0/+
White matter	0/+	0/++	0/++	0/+	0/+	0/+	0/++	0/+
Dentate nucleus	++	+	0/++	0/+	0/++	0/+	0/++	0/+
Corpus amygdaloideum								
Lateral nucleus	0/+++	0/++	0/++	0/+	0/+++	0/+	0/++	0/+
Basomedial nucleus	0/++	0/+	0/++	0/+	+/++	+	0/++	0/+
Basolateral nucleus	++	+	+/++	+	++	+	0/++	0/+

Density: 0: no immunoreactive structures, + up to 10%, ++ 10–50%, +++ more than 50%. Intensity: 0: no immunoreactivity, + faint, ++ moderate, +++ strong. The range of minimum and maximum staining between individual cases is given.

(Fig. 1). Nearly all cells of the choroid plexus revealed moderate staining intensities.

Spatial distribution of G-CSF R IR

Cerebral cortex

G-CSF R IR in cortical neurons with pyramidal morphology was largely restricted to scattered faintly stained cells in layer III in Wernicke's area, whereas no immunostained pyramidal neurons were present in the remaining cortical regions investigated (Fig. 3; cf. Tables 7–10). Non-pyramidal slightly stained neurons were almost exclusively detectable in layer I of all cortical regions analyzed. Neuropil staining was only faint.

Hippocampus

The pyramidal neurons in the hippocampal subfields CA2 and CA3 as well as the hilar neurons were weakly labeled

Table 5 Distribution of G-CSF IR in the brainstem.

	Control				AD			
	Neuronal cell bodies		Fibers		Neuronal cell bodies		Fibers	
	Density	Intensity	Density	Intensity	Density	Intensity	Density	Intensity
Brain stem								
Oculomotor nucleus	+++	+/++	0/++	0/+	0/+++	0/++	0/++	0/+
Trochlear nucleus	++/+++	+/++	0/+++	0/++	0/+++	0/++	0/++	0/+
Pontine nuclei	0/++	0/+	0/++	0/+	0/++	0/++	0/++	0/+
Locus caeruleus	0	0	0	0	0	0	0/++	0/+
Mesencephalic nucleus	0/++	0/++	0/++	0/+	0/++	0/+	0/++	0/+
Dorsal raphe nucleus	++	+/++	0/++	0/+	0/+++	0/++	0/+++	0/+
Facial motor nucleus	+++	+/++	++	+	0/+++	0/++	0/++	0/+
Superior salivatory nucleus	0/+++	0/+	0	0	0/++	0/++	0	0
Abducens nucleus	++/+++	+/++	0/++	0/+	++	+	+/++	+
Superior olivary nucleus	0	0	++	+	0	0	0	0
Inferior olivary nucleus	++/+++	+/++	++	+	++/+++	+	+/++	+
Accessory olivary nucleus	++/+++	+/++	++	+	++/+++	+/++	0/+	0/+
Arcuate nucleus	0/+++	0/+	0/+++	0/+	0/++	0/+	+/++	+
Nucleus ambiguus	0/+++	0/+	0/++	0/+	++	+	0	0
Nucleus of solitary tract	++/+++	+	++	+	0/+++	0/+	0/++	0/+
Spinal tigeminal nucleus	++	+	0/++	0/++	0/++	0/+	0/++	0/+
Trigeminal motor nucleus	++/+++	+	0	0	0/+++	0/+	0/++	0/+
Hypoglossal nucleus	++/+++	+/++	0/++	0/+	++/+++	+/++	0/++	0/+
Dorsal motor nucleus of vagus	++	+/++	0/+++	0/+	0/++	0/++	0/++	0/+
Inferior vestibular nucleus	++/+++	+/++	++	+	++	+	0/++	0/+
Medial vestibular nucleus	++	+/++	0/++	0/+	0/++	0/++	0/++	0/+
Gracile nucleus	0/+++	0/++	++	+	0/++	0/+	0/++	0/++
Cuneate nucleus	0/++	0/++	0/+++	0/+	0/++	0/+	+/++	+

Density: 0: no immunoreactive structures, + up to 10%, ++ 10–50%, +++ more than 50%. Intensity: 0: no immunoreactivity, + faint, ++ moderate, +++ strong. The range of minimum and maximum staining between individual cases is given.

Table 6 Distribution of G-CSF IR in non-neuronal cells of the CNS.

	Control				AD			
	Cell bodies		Fibers		Cell bodies		Fibers	
	Density	Intensity	Density	Intensity	Density	Intensity	Density	Intensity
Astrocytes	++	+/++	–	–	++	++	–	–
Choroid plexus	0/+++	0/++	–	–	++/+++	++	–	–
Ependyma	0/++	0/++	–	–	0/++	0/+	–	–

Density: –: not done; 0: no immunoreactive structurs, + up to 10%, ++ 10–50%, +++ more than 50%. Intensity: –: not done; 0: no immunoreactivity, + faint, ++ moderate, +++ strong. The range of minimum and maximum staining between individual cases is given.

with the G-CSF R antiserum. However, there was distinct variation in staining intensity between the individual cases. CA1 pyramidal cells and granule cells of the dentate gyrus remained largely unstained. Neuropil staining in these regions was only weak. Whereas the neurons of the entorhinal cortex showed faint staining, the neurons of the subiculum were completely unlabeled. Neuropil staining was weak in both regions. In the lateral geniculate nucleus, most neurons were labeled and exhibited distinct cytoplasmic staining for G-CSF R (Fig. 4).

Basal ganglia

Within the putamen, neuronal IR was mostly restricted to large slightly stained neurons. Small neurons were almost unstained. The neuropil was faintly labeled in both putamen and caudate nucleus. However, some fiber bundles

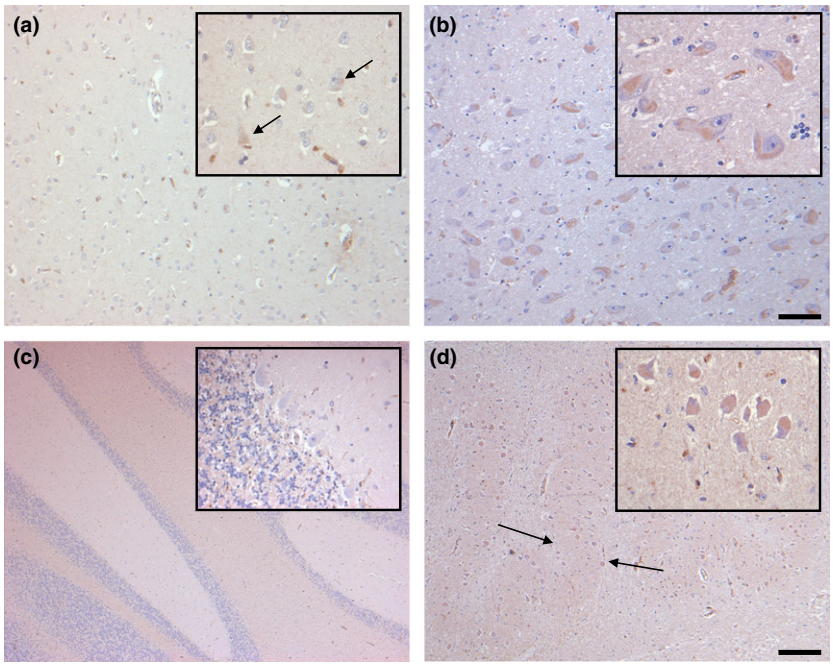

Fig. 2 Distribution of G-CSF IR in the inferior temporal gyrus (a), the basal nucleus of Meynert (b), the cerebellum (c) and the inferior olivary nucleus (d) of controls. Some scattered cortical neurons of the inferior temporal gyrus display faint immunostaining (a, arrows). By contrast, nearly all neurons of the basal nucleus of Meynert are labeled, although IR is only faint (b). In the cerebellum, G-CSF IR is largely absent (c). In the inferior olivary nucleus, all neurons and the neuropil (arrows) are faintly stained (d). Sections are counterstained with hematoxylin. Scale bars: 50 μm (all insets), 100 μm (a,b), and 400 μm (c,d), respectively.

stained more intensely. Within the pallidum, the neuropil disclosed a moderate staining intensity, whereas the neurons in this region remained unstained.

Thalamus and hypothalamus

Faint neuronal IR was noted in the ventral lateral nucleus as well as in the medial and lateral pulvinar, whereas the remaining nuclei did not show any labeled neurons. Similarly, the neuropil revealed weak immunostaining only in nuclei with immunoreactive neurons. Faint IR was present in the hypothalamic neurons as well as in the surrounding neuropil of the supraoptic nucleus, whereas the paraventricular and dorsomedial nuclei were nearly completely devoid of immunostained neurons.

Claustrum and nucleus basalis of Meynert

Within the claustrum, no immunoreactive neurons were detectable but a few weakly stained fibers were present. In the nucleus basalis of Meynert, the majority of large neurons were faintly labeled. Only a small portion of fibers in this region was slightly to moderately stained (Fig. 3).

Amygdala

All three amygdaloid nuclei analyzed were devoid of G-CSF receptor-positive neurons, whereas the neuropil was weakly stained.

Cerebellum

Cerebellar Purkinje cells and neurons of the molecular layer as well as the surrounding neuropil were devoid of immunoreactivity. The granule cell layer exhibited faintly stained neurons. The dentate nucleus showed a moderate density of faintly labeled neurons. In the white matter, some cell bodies were slightly labeled. Neuropil staining in the white matter, the dentate nucleus, and the granular layer was weak.

Brainstem

The neuromelanin-containing neurons of the substantia nigra, surrounded by slightly labeled fibers, did not display any G-CSF IR. Neurons of the red nucleus remained unstained, but there was a high density of moderately labeled fibers in this region. Only weak IR could be observed in neurons and fibers of the mammillary bodies.

The oculomotor and trochlear nuclei showed a low to moderate density of moderately stained neuronal cell bodies and slightly stained fibers.

In the pons, neurons and fibers were faintly labeled. Neurons of the locus coeruleus were embedded in faintly labeled fibers and did not show any IR. The motor neurons in the facial nucleus as well as the motor neurons of the motor trigeminal nucleus did not show any IR either, but were embedded in a slightly labeled neuropil.

Table 7 Distribution of G-CSF R IR in cortical regions.

	Control				AD			
	Neuronal cell bodies		Fibers		Neuronal cell bodies		Fibers	
	Density	Intensity	Density	Intensity	Density	Intensity	Density	Intensity
Cerebral cortex								
Wernicke's area								
I	++	+	+/++	+	+/++	+	0/+	0/+
II	0	0	+/++	+	0	0	0/+	0/+
III	0/+++	0/+	+/++	+	0/+++	0/++	0/+	0/+
IV	0	0	+/++	+	0	0	0/+	0/+
V	0	0	+/++	+	0/++	0/+	0/+	0/+
VI	0	0	+/++	+	0	0	0/+	0/+
Frontal pole								
I	++	+	+/++	+	+/++	+	0/+	0/+
II	0	0	+/++	+	0	0	0/+	0/+
III	0	0	+/++	+	0	0	0/+	0/+
IV	0	0	+/++	+	0	0	0/+	0/+
V	0	0	+/++	+	0	0	0/+	0/+
VI	0	0	+/++	+	0	0	0/+	0/+
Occipital pole								
I	++	+	+/++	+	+	+	0/+	0/+
II	0	0	+/++	+	0	0	0/+	0/+
III	0	0	+/++	+	0	0	0/+	0/+
IV	0/+	0/+	+/++	+	0	0	0/+	0/+
V	0	0	+/++	+	0	0	0/+	0/+
VI	0	0	+/++	+	0	0	0/+	0/+
Inferior temporal gyrus								
I	+/++	+	+/++	+	+/++	+	0/+	0/+
II	0	0	+/++	+	0/+	0/+	0/+	0/+
III	0	0	+/++	+	0/+++	0/+	0/+	0/+
IV	0	0	+/++	+	0/+	0/+	0/+	0/+
V	0	0	+/++	+	0/++	0/+	0/+	0/+
VI	0	0	+/++	+	0/+	0/+	0/+	0/+
Cingulate gyrus								
I	++	+	0/+	0/+	++	+	0/+	0/+
II	0	0	+	+	0	0	0/+	0/+
III	0	0	+	+	0	0	0/+	0/+
IV	0	0	+	+	0	0	0/+	0/+
V	0	0	+	+	0	0	0/+	0/+
VI	0	0	+	+	0	0	0/+	0/+

Density: 0: no immunoreactive structurs, + up to 10%, ++ 10–50%, +++ more than 50%. Intensity: 0: no immunoreactivity, + faint, ++ moderate, +++ strong. The range of minimum and maximum staining between individual cases is given.

Within the inferior olivary complex, weak IR could be observed in many neuronal cell bodies surrounded by slightly stained neuropil (Fig. 3). The nucleus of the solitary tract did not reveal any IR, whereas fibers were barely stained. In the spinal trigeminal nucleus, numerous faintly labeled neurons were present and embedded in weakly stained fibers.

A high density of faintly labeled neurons surrounded by weakly labeled fibers could also be observed in the hypoglossal nucleus. Within the vestibular nuclei, slightly to moderately stained neurons could be detected. Surrounding fibers were also only weakly stained.

G-CSF R IR in the brains of AD patients vs. controls

Similar to G-CSF, there were no significant differences in the pattern and intensity of G-CSF R IR between brains of AD patients and the respective controls (cf. Tables 7–10). Again, there was some variation in staining intensity in all brain regions with predominant neuronal or neuropil staining, sometimes in control brains, sometimes in AD brains. Focusing on the hippocampus as a target region of AD, no differences were detectable between the groups. Neurofibrillary tangles and amyloid plaques, representing the specific histopathological hallmarks in AD, did not show any IR

Table 8 Distribution of G-CSF R IR in non-cortical areas of the forebrain.

	Control				AD			
	Neuronal cell bodies		Fibers		Neuronal cell bodies		Fibers	
	Density	Intensity	Density	Intensity	Density	Intensity	Density	Intensity
Basal ganglia								
Claustrum	0	0	0/+	0/+	0	0	0/+	0/+
Putamen	0/+	0/+	0	0	0	0	0/+	0/+
Pallidum	0	0	0/++	0/++	0/++	0/+	0/+	0/+
Caudate nucleus	0	0	0/+	0/+	0	0	0/+	0/+
Basal nucleus of Meynert	0/++	0/+	+	+/++	0/++	0/+	0/+	0/++
Hippocampus								
Dentate gyrus	0	0	+	+	0/+	0/+	0/++	0/+
Hilus	0/+++	0/+	0/+	0/+	0/+++	0/++	0/+	0/+
CA3	0/+++	0/+	0/+	0/+	0/++	0/+	0/+	0/+
CA2	0/+++	0/+	0/++	0/+	0/++	0/+	0/++	0/+
CA1	0	0	0/+	0/+	0/+	0/+	0/+	0/+
Subiculum	0	0	0/+	0/+	0/+	0/+	0/++	0/+
Entorhinal cortex	0/++	0/+	0/++	0/+	0/++	0/++	0/++	0/+
Lateral geniculate nucleus	0/+++	0/+++	+/++	+	0/+	0/+	0/+	0/+
Thalamus								
Anterior nucleus	0	0	+/++	+/++	0/+++	0/++	0/+	0/+
Ventral anterior nucleus	0	0	+	+/++	0/+++	0/++	0/+	0/+
Ventral lateral nucleus	0/++	0/+	0/+++	0/++	0/++	0/++	0/+	0/+
Dorsomedial nucleus	0	0	0/++	0/++	0/++	0/++	0/+	0/+
Subthalamic nucleus	0	0	0/++	0/++	0/+	0/+	0/++	0/+
Pulvinar medial	0/++	0/+	+	+	0/++	0/++	0/+	0/+
Lateral	0/++	0/+	+	+	0/++	0/++	0/+	0/+
Hypothalamus								
Paraventricular nucleus	0	0	0/+	0/+	0	0	+	+
Supraoptic nucleus	0/+++	0/+	++/+++	+	0/++	0/+	0/+	0/+
Dorsomedial nucleus	0	0	+	+	0/++	0/+	0/+	0/+
Substantia nigra	0	0	+	+	0	0	0/++	0/+
Nucleus ruber	0	0	0/+++	0/++	0/+++	0/++	0/++	0/+
Mamillary bodies	0/+	0/+	0/++	0/+	0/+++	0/+	0/+	0/+
Cerebellum								
Purkinje layer	0	0	–	–	0	0	–	–
Molecular layer	0	0	+	+	0/+	0/+	0/+	0/++
Granular layer	+	+	0/++	0/+	0/+	0/+	0/+	0/+
White matter	++	+	0/+	0/+	+/++	+	0/+	0/+
Dentate nucleus	++	+	+	+	++/+++	+	0/+	0/++
Corpus amygdaloideum								
Lateral nucleus	0	0	+	+	0	0	+	+
Basomedial nucleus	0	0	+	+	0/+	0/+	+	+
Basolateral nucleus	0	0	+	+	0/+	0/+	+	+

Density: 0: no immunoreactive structures, + up to 10%, ++ 10–50%, +++ more than 50%. Intensity: 0: no immunoreactivity, + faint, ++ moderate, +++ strong. The range of minimum and maximum staining between individual cases is given.

for either G-CSF or its receptor (Fig. 4). Neurons containing neurofibrillary tangles did not reveal any difference in staining compared with surrounding neurons devoid of tangles. As to the various cell types, the level of intensity concerning astrocytic, ependymal, and choroid plexus immunostaining was largely similar in AD brains compared with controls.

Discussion

Our study has, for the first time, systematically analyzed the distribution of G-CSF and its receptor using immunohistochemistry in the adult human brain. Furthermore, we checked for potential alterations in the abundance of the G-CSF system in brains from AD patients. The main findings

Table 9 Distribution of G-CSF R IR in the brainstem.

	Control				AD			
	Neuronal cell bodies		Fibers		Neuronal cell bodies		Fibers	
Brain stem	Density	Intensity	Density	Intensity	Density	Intensity	Density	Intensity
Oculomotor nucleus	0/+	0/++	0/+	0/+	0/+	0/+	0/+	0/+
Trochlear nucleus	+/++	+/++	0/+	0/+	++	+/++	0/+	0/+
Pontine nuclei	0/+	0/+	0/+	0/+	0/++	0/+	0/+	0/+
Locus caeruleus	0	0	0/+	0/+	0/+	0/++	0/+	0/+
Mesencephalic nucleus	0/++	0/+	0/+	0/+	0/+++	0/+	0/+	0/+
Dorsal raphe nucleus	0	0	0/++	0/+	0	0	0/+	0/+
Facial motor nucleus	0	0	0	0	0/+	0/+	0/++	0/+
Superior salivatory nucleus	0	0	0/+	0/+	0	0	0/+	0/+
Abducens nucleus	0/+	0/+	0/++	0/+	0/++	0/+	0/++	0/+
Superior olivary nucleus	0/+	0/+	0	0	0	0	0/+	0/+
Inferior olivary nucleus	0/++	0/+	+	+	0/+	0/+	0/+	0/+
Accessory olivary nucleus	0/+	0/+	+	+	0	0	0/++	0/+
Arcuate nucleus	0	0	+	+/++	0/++	0/+	+/++	+
Nucleus ambiguus	0/++	0/+	0/+	0/+	0/+++	0/++	0/+	0/+
Nucleus of solitary tract	0	0	0/+	0/+	0	0	0/+	0/+
Spinal trigeminal nucleus	0/++	0/+	+	+	0/+	0/+	0/+	0/+
Trigeminal motor nucleus	0	0	0/+	0/+	0	0	0/+	0/+
Hypoglossal nucleus	0/+++	0/+	0/++	0/+	0/+++	0/++	0/+	0/+
Dorsal motor nucleus of vagus	0/+	0/+	+	+	0	0	0/+	0/+
Inferior vestibular nucleus	++/+++	+/++	0/++	0/+	0/++	0/+	0/++	0/+
Medial vestibular nucleus	0/++	0/++	0/++	0/+	0/++	0/+	0/+	0/+
Gracile nucleus	0/++	0/++	+	+	0/+++	0/+	0/++	0/+
Cuneate nucleus	0/++	0/++	+	+	0/++	0/+	0/+	0/+

Density: 0: no immunoreactive structures, + up to 10%, ++ 10–50%, +++ more than 50%. Intensity: 0: no immunoreactivity, + faint, ++ moderate, +++ strong. The range of minimum and maximum staining between individual cases is given.

Table 10 Distribution of G-CSF R IR in non-neuronal cells of the CNS.

	Control				AD			
	Cell bodies		Fibers		Cell bodies		Fibers	
	Density	Intensity	Density	Intensity	Density	Intensity	Density	Intensity
Astrocytes	+++	+/++	–	–	++/+++	+/++	–	–
Choroid plexus	+++	++	–	–	+++	++	–	–
Ependyma	++	+/++	–	–	++/+++	+/++	–	–

Density: –: not done; 0: no immunoreactive structures, + up to 10%, ++ 10–50%, +++ more than 50%. Intensity: –: not done; 0: no immunoreactivity, + faint, ++ moderate, +++ strong. The range of minimum and maximum staining between individual cases is given.

can be summarized as follows: (i) both G-CSF and G-CSF R are ubiquitously but not uniformly expressed in neurons throughout the CNS; (ii) G-CSF and G-CSF R IR is also detectable in glial cells, ependymal cells, and cells of the choroid plexus; (iii) neither pattern nor intensity of IR for G-CSF or G-CSF R differed in brains from AD patients compared with controls.

G-CSF and G-CSF R are ubiquitously but not uniformly expressed in neurons throughout the CNS

Knowledge about the distribution of G-CSF and its receptor in the human brain is still restricted to a few reports primarily focusing on the expression patterns of these proteins after ischemic stroke. While upregulation of

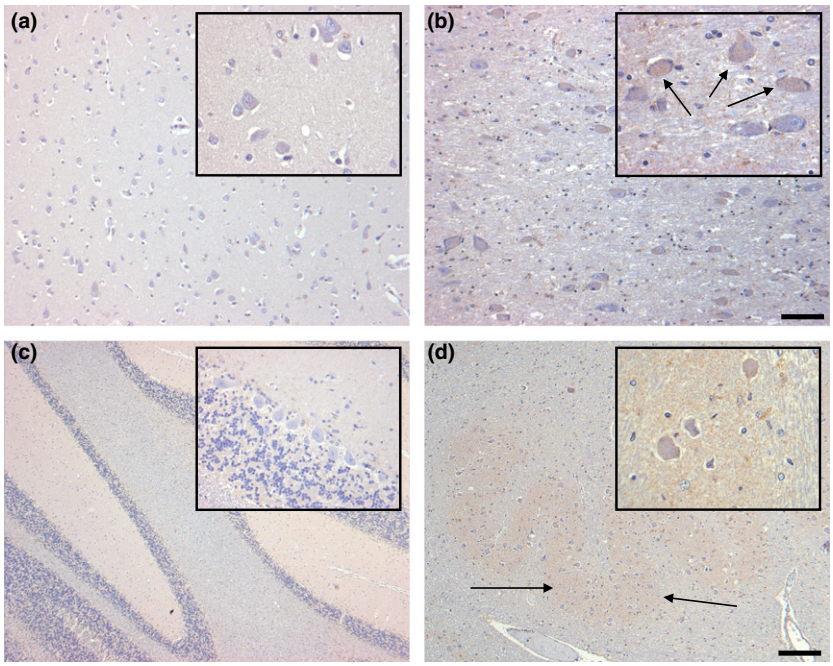

Fig. 3 Distribution of G-CSF R IR in the inferior temporal gyrus (a), the basal nucleus of Meynert (b), the cerebellum (c) and the inferior olivary nucleus (d) of controls. Pyramidal neurons of the inferior temporal gyrus display no immunostaining (a). Scattered neurons of the basal nucleus of Meynert are faintly labeled (b). Within the cerebellar cortex, only weak immunostaining is visible in the granule cell layer (c). In the inferior olivary nucleus, neurons are very weakly labeled, while faint staining is visible in the neuropil (d, arrows). Sections are counterstained with hematoxylin. Scale bar: 50 μm (all insets), 100 μm (a,b) and 400 μm (c,d), respectively.

both G-CSF R and its ligand G-CSF – in particular within the peri-infarct tissue – could be clearly demonstrated in these studies, neuronal IR on the contralateral side and in control subjects was considered to be only weak (Schneider et al. 2005; Hasselblatt et al. 2007). Our present results substantially extend these limited findings, demonstrating that both G-CSF and G-CSF R IR are present in neurons throughout the forebrain, cerebellum, and brain stem, albeit with different staining intensity. In general, G-CSF and G-CSF R IR were most prominent in many brain stem nuclei as well as in specific nuclei within the forebrain, whereas cortical and hippocampal protein expression was only weak. Within the cerebellum, only small neurons showed immunohistochemical staining, whereas Purkinje cells were completely devoid of G-CSF R IR and stained very slightly for G-CSF. This spatial pattern of G-CSF and G-CSF R IR in humans is in general accordance with those findings originating from rats, at least as far as the analysis of the distribution of this hematopoeitic growth factor and its receptor are concerned (Schäbitz et al. 2003; Schneider et al. 2005). However, there are exceptions, such as the distinct labeling of Purkinje cells for G-CSF R within the cerebellum of the rat compared with the complete lack of G-CSF R IR for these cells within the human brain (Schneider et al. 2005). Furthermore, although expression of the G-CSF R has convincingly been demonstrated in dopaminergic cells in the substantia nigra of mice and rats (Cao et al. 2006; Meuer et al. 2006), in our present study both G-CSF and its receptor could not be detected in human brain substantia nigra by immunohistochemistry. In general, however, G-CSF and its receptor are widely expressed throughout the CNS, thus making it an interesting candidate for treatment of various acute and chronic degenerative diseases.

G-CSF and G-CSF R IR are also detectable in glial cells, ependymal cells, and cells of the choroid plexus

Expression of G-CSF and its receptor in glial cells has already been described in rodents and humans (Schäbitz et al. 2003; Hasselblatt et al. 2007) and, recently, the presence of G-CSF R in radial glia during development in the rat brain was demonstrated (Kirsch et al. 2008). Our present data corroborate these former findings by demonstrating glial IR for G-CSF and G-CSF R throughout the CNS. Although most of the previous studies of the protective effects of G-CSF after experimental brain ischemia in rodents have focused on neurons (Minnerup et al. 2008), there is now also evidence of postischemic activation concerning anti-apoptotic pathways in astrocytes (Solaroglu et al. 2006). Since these cells are not only essential for trophic support of neurons but also play a key role in conferring resistance against injury (Nedergaard & Dirnagl, 2005), G-CSF-induced survival

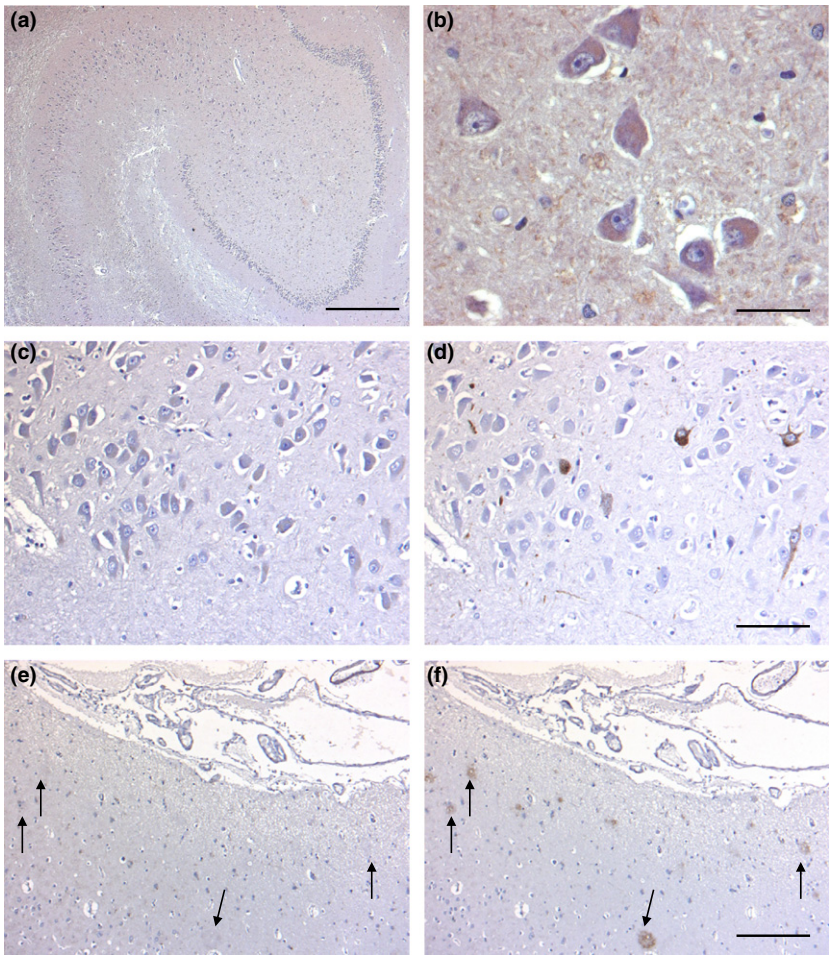

Fig. 4 Hippocampal distribution of G-CSF R IR in the hippocampus of control cases (a,b) and AD brains (c,d). At low magnification, no reliable IR is visible in the hippocampal formation (a). At higher magnification, very weakly stained hilar neurons are detectable (b). In consecutive sections from an AD brain, immunostaining for G-CSF R (c) and AT8 (d) clearly demonstrates that phospho-tau-positive neuronal structures are not labeled by antibodies recognizing G-CSF R. Similarly, amyloid plaques labeled with an anti-β-amyloid antibody (f, arrows) do not stain for G-CSF R (e, arrows). Sections are counterstained with hematoxylin. Scale bar: 50 μm (b), 100 μm (c,d), 200 μm (e,f), 400 μm (a).

of astrocytes may indirectly protect those neurons showing no or weak G-CSF R expression. Furthermore, coexpression of both the ligand and its receptor are highly suggestive of an autocrine loop of action.

To our knowledge, protein expression of G-CSF and G-CSF R by ependymal cells has not been reported up to now. The same holds true for the detection of distinct immunostaining for G-CSF and G-CSF R in cells of the choroid plexus. Although no functional data are available so far on a possible role of G-CSF concerning ependymal or choroid plexus cells, other growth factors, such as the vascular endothelial growth factor (VEGF) and the transforming growth factor beta (TGF-β), have been shown to be expressed by the choroid plexus and ependyma and have proved to be essential for the functionality and maintenance of these cells in mice (Maharaj et al. 2008). Therefore, the strong protein expression demonstrated by immunohistochemistry suggests an important role also of the G-CSF system within this cell system; this, however, remains to be clarified by more detailed future experiments.

Neither pattern nor intensity of IR for G-CSF or G-CSF R differed in brains from AD patients compared with controls

Using a transgenic model of G-CSF-deficient mice, the important physiological role of G-CSF for memory formation and structural integrity of the hippocampal formation has recently been demonstrated (Diederich et al. 2009). Since patients with early AD develop decreased G-CSF plasma levels, a link between trophic support from this growth factor and cognitive performance has been suggested (Laske et al. 2009). This view is supported by experiments with AD transgenic mice demonstrating a strong association between long-term treatment with coffee, which protected against cognitive decline and increased

plasma levels of G-CSF (Cao et al. 2011). In this context it would be reasonable to assume that a decline of G-CSF expression in AD at least in brain areas involved early on in neurodegenerative processes and cognitive decline such as the hippocampal formation may contribute to the progression of the disease. This hypothesis is further corroborated by transgenic mouse models of AD where treatment with G-CSF has been shown to reduce amyloid burden and to reverse cognitive impairment (Tsai et al. 2007; Sanchez-Ramos et al. 2009). Apart from indirect effects via the hematopoietic system, the G-CSF effect may also have been mediated by direct interaction with central G-CSF Rs because G-CSF is able to pass the intact blood-brain barrier (Schneider et al. 2005). Concerning this issue, it was extremely interesting to check for potential changes in the abundance of G-CSF Rs, which are a prerequisite for direct G-CSF effects in the CNS. Surprisingly, no distinct differences were detectable concerning the protein expression of G-CSF R or its ligand G-CSF when comparing AD brains with those of controls. This is even more remarkable since the patients in the AD group were considerably older than the controls and an age-related decrease in G-CSF production might have been suspected to mimic AD-related effects. Since all the brains from AD patients used in the present study were categorized as Braak staging III/IV, a potential impact of this neurodegenerative disease on the expression of G-CSF or its receptor at least in the hippocampus and entorhinal cortex could have to be expected. The absence of substantial differences in G-CSF or G-CSF R protein expression can also not be explained by a false result due to differing neuronal cell densities because an analysis of neuronal cell numbers in the stage-defining regions of AD revealed no significant differences (Table 2). In contrast to other growth factors, such as BDNF, VEGF or GM-CSF (Murer et al. 1999; Yang et al. 2004; Ridwan et al. 2012), tangles and plaques were also devoid of both G-CSF and its receptor. Although the number of cases analyzed in our present study was rather small due to the fact that it was primarily designed to obtain as much information as possible on the exact distribution of G-CSF and its receptor throughout the human CNS, our data suggest that further experiments are mandatory to decipher the role of the G-CSF system in AD.

Acknowledgements

This work contains parts of the thesis by Sami Ridwan. The authors kindly acknowledge the excellent technical support by Ralf Luderschmidt and Magdeleine Herkt. Furthermore, the authors would like to thank Astrid Wöber for her superb editorial assistance.

Authors' contributions

S.R.: Conception and design of the study, acquisition, analysis and interpretation of data, drafting the article; H.B.: Acquisition of data; K.F.: Acquisition of data, critically revising for important intellectual content; K.H.: Acquisition of data; H.v.P.: Acquisition of data, critically revising for important intellectual content; C.J.S.: Conception and design of the study, interpretation of data, final approval.

Conflict of interest

C.J.S. is an inventor on the patent application 'Hematopoietic factors for the treatment of neurological conditions'. Recently, a part of the patent application (ALS) has been accepted. C.J.S. transferred his rights to Sygnis Bioscience GmbH & Co. KG and received a minor financial compensation up-front.

References

Braak H, Alafuzoff I, Arzberger T, et al. (2006) Staging of Alzheimer disease-associated neurofibrillary pathology using paraffin sections and immunocytochemistry. *Acta Neuropathol* **12**, 389–404.

Cao X-Q, Arai H, Ren Y-R, et al. (2006) Recombinant human granulocyte colony-stimulating factor protects against MPTP-induced dopaminergic cell death in mice by altering Bcl-2/Bax expression levels. *J Neurochem* **99**, 861–867.

Cao C, Wang L, Lin X, et al. (2011) Caffeine synergizes with another coffee component to increase plasma G-CSF: linkage to cognitive benefits in Alzheimer's mice. *J Alzheimer's Dis* **25**, 323–335.

Diederich K, Sevimli S, Dörr H, et al. (2009) The role of granulocyte-colony stimulating factor (G-CSF) in the healthy brain: a characterization of G-CSF-deficient mice. *J Neurosci* **29**, 11572–11581.

Goedert M, Jakes R, Vanmechelen E (1995) Monoclonal antibody AT8 recognises tau protein phosphorylated at both serine 202 and threonine 205. *Neurosci Lett* **189**, 167–169.

Hasselblatt M, Jeibmann A, Riesmeier B, et al. (2007) Granulocyte-colony stimulating factor (G-CSF) and G-CSF receptor expression in human ischemic stroke. *Acta Neuropathol* **113**, 45–51.

Hennigan A, O'Callaghan RM, Kelly AM (2007) Neurotrophins and their receptors: roles in plasticity, neurodegeneration and neuroprotection. *Biochem Soc Trans* **35**, 424–427.

Kirsch F, Krüger C, Schneider A (2008) The receptor for granulocyte-colony stimulating factor (G-CSF) is expressed in radial glia development of the nervous system. *BMC Dev Biol* **8**, 32.

Laske C, Stellos K, Stransky E, et al. (2009) Decreased plasma levels of granulocyte-colony stimulating factor (G-CSF) in patients with early Alzheimer's disease. *J Alzheimer's Dis* **17**, 115–123.

Maharaj AS, Walshe TE, Saint-Geniez M, et al. (2008) VEGF and TGF-β are required for the maintenance of the choroid plexus and ependyma. *J Exp Med* **205**, 491–501.

Maurer MH, Schäbitz WR, Schneider A (2008) Old friends in new constellations – the hematopoietic growth factors G-CSF, GM-CSF, and EPO for the treatment of neurological diseases. *Curr Med Chem* **15**, 1407–1411.

Mercken M, Vandermeeren M, Lübke U, et al. (1992) Monoclonal antibodies with selective specificity for Alzheimer tau are directed against phosphatase-sensitive epitopes. *Acta Neuropathol* **84**, 265–272.

Meuer K, Pitzer C, Teismann P, et al. (2006) Granulocyte-colony stimulating factor is neuroprotective in a model of Parkinson's disease. *J Neurochem* **97**, 675–686.

Minnerup J, Heidrich J, Wellmann J, et al. (2008) Meta-analysis of the efficacy of granulocyte-colony stimulating factor in animal models of focal cerebral ischemia. *Stroke* **39**, 1855–1861.

Murer MG, Boissiere F, Yan Q, et al. (1999) An immunohistochemical study of the distribution of brain-derived neurotrophic factor in the adult human brain, with particular reference to Alzheimer's disease. *Neuroscience* **88**, 1015–1032.

Nedergaard M, Dirnagl U (2005) Role of glial cells in cerebral ischemia. *Glia* **50**, 281–286.

Ridwan S, Bauer H, Frauenknecht K, et al. (2012) Distribution of granulocyte-monocyte colony-stimulating factor and its receptor α-subunit in the adult human brain with specific reference to Alzheimer's disease. *J Neural Transm* **119**, 1389–1406.

Sanchez-Ramos J, Song S, Sava V, et al. (2009) Granulocyte colony stimulating factor decreases brain amyloid burden and reverses cognitive impairment in Alzheimer's mice. *Neuroscience* **163**, 55–72.

Schäbitz WR, Kollmar R, Schwaninger M, et al. (2003) Neuroprotective effect of granulocyte colony-stimulating factor after focal cerebral ischemia. *Stroke* **34**, 745–751.

Schneider A, Krüger C, Steigleder T, et al. (2005) The hematopoietic factor G-CSF is a neuronal ligand that counteracts programmed cell death and drives neurogenesis. *J Clin Invest* **115**, 2083–2098.

Solaroglu I, Tsubokawa T, Cahill J, et al. (2006) Anti-apoptotic effect of granulocyte-colony stimulating factor after focal cerebral ischemia in the rat. *Neuroscience* **143**, 965–974.

Tsai K-J, Tsai Y-C, Shen C-KJ (2007) G-CSF rescues the memory impairment of animal models of Alzheimer's disease. *J Exp Med* **204**, 1273–1280.

Yang S-P, Bae D-G, Kang HJ, et al. (2004) Co-accumulation of vascular endothelial factor with β-amyloid in the brain of patients with Alzheimer's disease. *Neurobiol Aging* **25**, 283–290.